

Transition phenomena in unstably stratified turbulent flows

M. Bukai,^{*} A. Eidelman,[†] T. Elperin,[‡] N. Kleeorin,[§] I. Rogachevskii,[¶] and I. Sapir-Katiraie^{**}
*The Pearlstone Center for Aeronautical Engineering Studies, Department of Mechanical Engineering,
Ben-Gurion University of the Negev, P.O.Box 653, Beer-Sheva 84105, Israel*
(Dated: September 3, 2019)

We study experimentally and theoretically transition phenomena caused by the external forcing from Rayleigh-Bénard convection with the large-scale circulation (LSC) to the limiting regime of unstably stratified turbulent flow without LSC whereby the temperature field behaves like a passive scalar. In the experiments we use the Rayleigh-Bénard apparatus with an additional source of turbulence produced by two oscillating grids located nearby the side walls of the chamber. When the frequency of the grid oscillations is larger than 2 Hz, the large-scale circulation (LSC) in turbulent convection is destroyed, and the destruction of the LSC is accompanied by a strong change of the mean temperature distribution. However, in all regimes of the unstably stratified turbulent flow the ratio $[(\ell_x \nabla_x T)^2 + (\ell_y \nabla_y T)^2 + (\ell_z \nabla_z T)^2] / \langle \theta^2 \rangle$ varies slightly (even in the range of parameters whereby the behaviour of the temperature field is different from that of the passive scalar). Here ℓ_i are the integral scales of turbulence along x, y, z directions, T and θ are the mean and fluctuating parts of the fluid temperature. At all frequencies of the grid oscillations we have detected the long-term nonlinear oscillations of the mean temperature. The theoretical predictions based on the budget equations for turbulent kinetic energy, turbulent temperature fluctuations and turbulent heat flux, are in agreement with the experimental results.

PACS numbers: 47.27.te, 47.27.-i

I. INTRODUCTION

Various aspects of formation of large-scale circulations (LSC) and other types of coherent structures in a turbulent convection at large Rayleigh numbers have been discussed in a number of studies for the atmospheric flows [1–4], laboratory experiments in the Rayleigh-Bénard apparatus [5–30] and direct numerical simulations [31–34]. A mean-field theory [4, 35, 36] has been proposed for the explanation of formation of coherent structures in turbulent convection. It is known from laboratory experiments and numerical simulations [7, 14, 15, 21] that the coherent structures in the Rayleigh-Bénard turbulent convection are not driven by the turbulent Reynolds stresses, associated with the tilting plumes at the upper and the lower horizontal walls. If the mean flow is established, the temperature of the fluid is larger at one side of the LSC and smaller at the other side of the LSC, and the mean flow is driven by the mean buoyancy force at the side walls of the chamber.

The effect of coherent structures (mean wind) on global properties of turbulent convection is a subject of numerous discussions (see, e.g., reviews [37–39]). It has been recently found in laboratory experiments in [40], that in turbulent convection with the mean wind the bulk

production of turbulence is due to the large-scale shear caused by the mean wind rather than by buoyancy.

Numerous experiments demonstrate that the mean temperature distribution in turbulent convection is strongly inhomogeneous and anisotropic due to the mean wind (see, e.g., [7, 15, 18, 21, 40]), and the mean temperature gradient in the horizontal direction inside the LSC can be significantly larger than in the vertical direction, i.e., the vertical turbulent heat flux inside the LSC is very small.

On the other hand, in a forced turbulent convection without a mean wind (i.e., in unstably stratified turbulent flows) the temperature field behaves like a passive scalar (see, e.g., [37, 41–43]). It is not clear why in turbulent convection with LSC the vertical gradient of the mean temperature field is small inside LSC, and the vertical temperature gradient can even change the direction, i.e., it can be directed upwards. A detailed study of a transition from one regime with mean wind to another regime without mean wind due to additional forcing in unstably stratified turbulent flow, can elucidate the effects of the mean wind on turbulent convection.

Different effects in turbulent convection with a forcing have been studied previously (see, e.g., [41, 44, 46, 47]). In particular, an experimental study of a turbulent convection with forcing in the form of periodical pulses has been performed in [44]. In these experiments, in spite of the forcing, a large-scale circulatory flow was not destroyed, and the heat transfer in this system was enhanced in comparison with constant and sinusoidally modulated energy inputs. It was found in [44] that the enhancement of the heat transfer depends on the synchronization of the kicking period of energy input with the intrinsic time scale of the turbulent flow. In other type of experiments [46, 47] a relation between convec-

^{*}Electronic address: mbukai@gmail.com

[†]Electronic address: eidel@bgu.ac.il

[‡]Electronic address: elperin@bgu.ac.il;

URL: <http://www.bgu.ac.il/me/staff/tov>

[§]Electronic address: nat@bgu.ac.il

[¶]Electronic address: gary@bgu.ac.il;

URL: <http://www.bgu.ac.il/~gary>

^{**}Electronic address: katiraie@bgu.ac.il

tive heat flux and temperature gradient was determined in a vertical channel filled with water, the average vertical mass flux being zero. It was shown in these experiments that when the LSC is suppressed by physically blocking its path, there exists a strong vertical temperature gradient in the bulk of the Rayleigh-Bénard apparatus and the temperature remains active, rather than passive field.

The goal of this paper is to study experimentally and theoretically transition phenomena due to the external forcing from Rayleigh-Bénard convection with LSC to the limiting regime of unstably stratified turbulent flow without LSC, whereby the temperature field behaves like a passive scalar. In the experimental study we use the Rayleigh-Bénard apparatus with an additional source of turbulence produced by the two oscillating grids located nearby the side walls of the chamber. Additional forcing for turbulence allows us to observe evolution of the mean temperature and velocity fields during the transition from pure turbulent convection with LSC (for very small frequencies of the grid oscillations) to the limiting regime of unstably stratified flow without LSC (for very high frequencies of the grid oscillations). We use Particle Image Velocimetry to determine the turbulent and mean velocity fields, and a specially designed temperature probe with sensitive thermocouples is employed to measure the temperature field.

Note that this experimental set-up with the turbulent convection and the external forcing has been previously used in studies of turbulent transport of particles (see, e.g., [45, 48–50]). Comprehensive investigation of turbulence structures, mean velocity and temperature distributions, velocity and temperature fluctuations can elucidate a complicated physics related to particle clustering and formation of large-scale inhomogeneities in particle spatial distributions in unstably stratified turbulent flows. Notably, turbulent convection with the external forcing is used in chemical industrial devices to improve mixing (see, e.g., [51–53]). Another example of turbulent convection with forcing is atmospheric wind superimposed on turbulent convective boundary layer.

The paper is organized as follows. Section II describes the experimental set-up, instrumentation and the results of laboratory study of the transition phenomena in unstably stratified turbulent flow. The theoretical analysis and comparison with the experimental results are performed in Section III. Finally, conclusions are drawn in Section IV. In Appendix we present the detailed derivations of the theoretical model for a passive scalar that used for the explanation of the observed effects.

II. EXPERIMENTAL STUDY

Let us start with description of the experimental set-up and the results of laboratory study of the transition phenomena in unstably stratified turbulent flow.

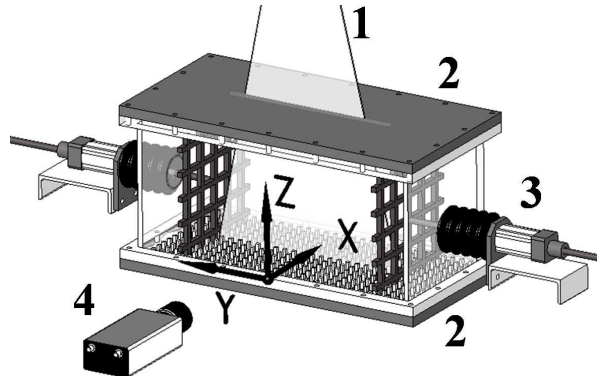


FIG. 1: Experimental set-up: (1) -laser light sheet; (2) - heat exchangers; (3) - grid driver; (4) - digital CCD camera.

A. Experimental set-up and instrumentation

The experiments on transition phenomena in unstably stratified turbulence have been conducted in rectangular chamber with dimensions $26 \times 58 \times 26 \text{ cm}^3$ in air flow with the Prandtl number $\text{Pr} = 0.71$. The side walls of the chambers are made of transparent Perspex with the thickness of 10 mm. In the experiments we use the Rayleigh-Bénard apparatus with an additional source of turbulence produced by two oscillating grids. Pairs of vertically oriented grids with bars arranged in a square array (with a mesh size 5 cm) are attached to the right and left horizontal rods (see Fig. 1). The grids are positioned at a distance of two grid meshes from the chamber walls and are parallel to the side walls. Both grids are operated at the same amplitude of 61 mm, at a random phase and at the same frequency varied in the range from 0.5 Hz to 16.5 Hz. Here we use the following system of coordinates: z is the vertical axis, the y -axis is perpendicular to the grids and the xz -plane is parallel to the grids.

A vertical mean temperature gradient in the turbulent air flow was formed by attaching two aluminium heat exchangers to the bottom and top walls of the test section (a heated bottom and a cooled top wall of the chamber). In order to improve heat transfer in the boundary layers at the bottom and top walls we used heat exchangers with rectangular fins $3 \times 3 \times 15 \text{ mm}^3$ (see Fig. 1) which allowed us to form a mean temperature gradient up to 115 K/m at a mean temperature of about 308 K when the frequency of the grid oscillations $f > 10 \text{ Hz}$. The thickness of the aluminium plates with the fins is 2.5 cm. The top plate is a bottom wall of the tank with cooling water. Temperature of water circulating through the tank and the chiller is kept constant within 0.1 K. Cold water is pumped into the cooling system through two inlets and flows out through two outlets located at the side wall

of the cooling system. The bottom plate is attached to the electrical heater that provides constant and uniform heating. The voltage of a stable power supply applied to the heater varies up to 200 V. The power of the heater varies up to 300 W.

The temperature field was measured with a temperature probe equipped with twelve E-thermocouples (with the diameter of 0.13 mm and the sensitivity of $\approx 65 \mu\text{V}/\text{K}$) attached to a vertical rod with a diameter 4 mm. The spacing between thermocouples along the rod was 22 mm. Each thermocouple was inserted into a 1 mm diameter and 45 mm long case. A tip of a thermocouple protruded at the length of 15 mm out of the case. The temperature was measured for 12 rod positions with 23 mm intervals in the horizontal direction, i.e., at 144 locations in a flow. The exact position of each thermocouple was measured using images captured with the optical system employed in PIV measurements. A sequence of 600 temperature readings for every thermocouple at every rod position was recorded and processed using the developed software based on LabView 7.0. Temperature maps and isothermal lines were plotted using Matlab 7. The temperature difference between the top and bottom plates, ΔT , in all experiments was 50 K (i.e., the global Rayleigh number based on molecular transport coefficients, was $\text{Ra} = 0.73 \times 10^8$).

In order to decrease mean flow generated by oscillating grids and to increase the range of homogeneous and isotropic turbulence we use partitions located in xz plane between grids and side walls of the chamber (of the width 85 mm). The aspect ratio of the chamber $A = H_y/H_z = 1.52$, where H_y is the size of the chamber along y -axis between partitions and H_z is the height of the chamber z -axis, respectively.

The velocity fields were measured using a Stereoscopic Particle Image Velocimetry (PIV), see [54–56]. In the experiments we used LaVision Flow Master III system. A double-pulsed light sheet was provided by a Nd-YAG laser (Continuum Surelite 2 \times 170 mJ). The light sheet optics includes spherical and cylindrical Galilei telescopes with tuneable divergence and adjustable focus length. We used two progressive-scan 12 bit digital CCD cameras (with pixel size $6.7 \mu\text{m} \times 6.7 \mu\text{m}$ and 1280×1024 pixels) with a dual-frame-technique for cross-correlation processing of captured images. A programmable Timing Unit (PC interface card) generated sequences of pulses to control the laser, camera and data acquisition rate. The software package LaVision DaVis 7 was applied to control all hardware components and for 32 bit image acquisition and visualization. This software package comprises PIV software for calculating the flow fields using cross-correlation analysis.

In order to obtain velocity maps in the central region of the flow in the cross-section parallel to the grids and perpendicular to a front view plane, we used one camera with a single-axis Scheimpflug adapter. The angle between the optical axis of the camera and the front view plane as well as the angle between the optical axis

and the probed cross-section was approximately 45 degrees. The perspective distortion was compensated using Stereoscopic PIV system calibration kit whereby the correction was calculated for a recorded image of a calibration plate. The corrections were introduced in the recorded in the probed cross-section images before their processing using a cross-correlation technique for determining velocity fields.

An incense smoke with sub-micron particles ($\rho_p/\rho \sim 10^3$), as a tracer was used for the PIV measurements. Smoke was produced by high temperature sublimation of solid incense grains. Analysis of smoke particles using a microscope (Nikon, Epiphot with an amplification of 560) and a PM-300 portable laser particulate analyzer showed that these particles have an approximately spherical shape and that their mean diameter is of the order of $0.7 \mu\text{m}$. The probability density function of the particle size measured with the PM300 particulate analyzer was independent of the location in the flow for incense particle size of $0.5 - 1 \mu\text{m}$. The maximum tracer particle displacement in the experiment was of the order of $1/4$ of the interrogation window. The average displacement of tracer particles was of the order of 2.5 pixels. The average accuracy of the velocity measurements was of the order of 4% for the accuracy of the correlation peak detection in the interrogation window of the order of 0.1 pixel (see, e.g., [54–56]).

We determined the mean and the r.m.s. velocities, two-point correlation functions and an integral scale of turbulence from the measured velocity fields. Series of 520 pairs of images acquired with a frequency of 1 Hz, were stored for calculating velocity maps and for ensemble and spatial averaging of turbulence characteristics. The center of the measurement region in yz -plane coincides with the center of the chamber. We measured velocity in a flow domain $256 \times 256 \text{ mm}^2$ with a spatial resolution of 1024×1024 pixels. This corresponds to a spatial resolution $250 \mu\text{m} / \text{pixel}$. The velocity field in the probed region was analyzed with interrogation windows of 32×32 or 16×16 pixels. In every interrogation window a velocity vector was determined from which velocity maps comprising 32×32 or 64×64 vectors were constructed. The mean and r.m.s. velocities for every point of a velocity map were calculated by averaging over 520 independent maps, and then they were averaged over space in the central region.

The two-point correlation functions of the velocity field were determined for every point of the central part of the velocity map (with 16×16 vectors) by averaging over 520 independent velocity maps, which yields 16 correlation functions in y and z directions. Then the two-point correlation function was obtained by averaging over the ensemble of these correlation functions. An integral scale of turbulence, ℓ , was determined from the two-point correlation functions of the velocity field. In the experiments we evaluated the variability between the first and the last 20 velocity maps of the series of the measured velocity field. Since very small variability was found, these tests

showed that 520 velocity maps contain enough data to obtain reliable statistical estimates. We found also that the measured mean velocity field is stationary.

The characteristic turbulence time in the experiments $\tau_z = 0.28 - 0.62$ seconds, while the characteristic time period for the large-scale circulatory flow (~ 10 s) is by 1.5 orders of magnitude larger than τ_z . These two characteristic times are much smaller than the time during which the velocity fields are measured (~ 600 s). The size of the probed region did not affect our results. Similar experimental set-up and data processing procedure were used previously in the experimental study of different aspects of turbulent convection [22, 40] and in [45, 48–50] for investigating a phenomenon of turbulent thermal diffusion [57, 58].

B. Experimental results

Let us start the analysis of the obtained experimental results from the dynamics of the mean velocity field. In Fig. 2 we show the mean flow patterns obtained in the experiments with unforced turbulent convection (Fig. 2a) and with forced turbulent convection at different frequencies of the grid oscillations (Figs. 2b and 2c). When the frequency of the grid oscillations is larger than 2 Hz, the large-scale circulation (LSC) in turbulent convection in the yz -plane is not observed (see Figs. 2b and 2c). On the other hand, a complicated mean flow of the spiral form in the xz -plane with a non-zero mean vorticity in the y direction exists when the frequencies of the grid oscillations $2 < f < 7$ Hz.

The destruction of the LSC is accompanied by a strong change of the mean temperature distribution. The distribution of the measured mean temperature field depends strongly on the frequency f of the grid oscillations (see Figs. 3-5). In particular, for the very low frequency f the thermal structure inside the LSC in turbulent convection is inhomogeneous and anisotropic. The hot thermal plumes concentrate at one side of LSC, and cold plumes accumulate at the opposite side of LSC [18, 40]. In the central part of the flow the vertical mean temperature gradient $\nabla_z T$ changes its sign depending on the frequency of the grid oscillations (see Fig. 3).

At all frequencies of the grid oscillations we have observed the long-term nonlinear oscillations of the mean temperature with the period that is of the order of 10 s. Due to these nonlinear oscillations we perform the sliding averaging of the instantaneous temperature over time of 3 s. In particular, in Fig. 6 we show time dependencies of the instantaneous temperature T^{tot} , the temperature fluctuations θ , the long-term variations of mean temperature $\delta T = T - \bar{T}$ and the long-term variations of the vertical mean temperature gradient $\delta(\nabla_z T) = \nabla_z T - \overline{\nabla_z T}$ due to the nonlinear oscillations of the mean temperature. The bar here denotes additional time averaging. In Figs. 3-5 we also show by triangles the amplitude of the nonlinear long-term oscillations of the gradients of the

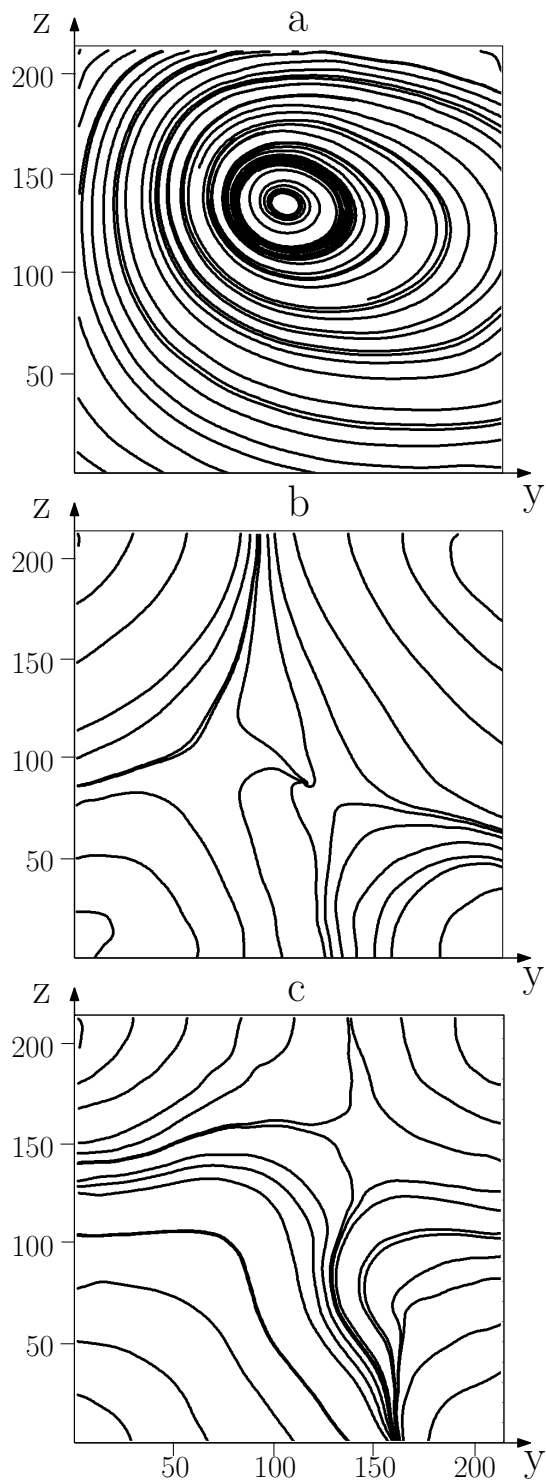


FIG. 2: Mean flow patterns obtained in the experiments with unforced turbulent convection (upper panel) and with forced turbulent convection at the frequencies $f = 2.2$ Hz (middle panel) and $f = 16.5$ Hz (lower panel) of the grid oscillations for the unstably stratified turbulent flow at the temperature difference between the top and bottom walls $\Delta T = 50$ K. Coordinates y and z are measured in mm.

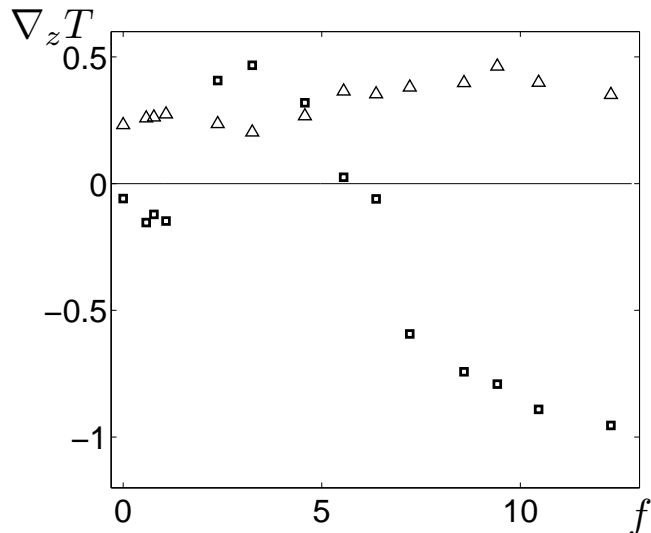


FIG. 3: Vertical gradient of the mean temperature $\nabla_z T$ (squares) and the amplitude of the nonlinear long-term oscillations of this gradient (triangles) versus the frequency f of the grid oscillations for the unstably stratified turbulent flow. The mean temperature gradient is measured in K cm^{-1} and the frequency f is measured in Hz.

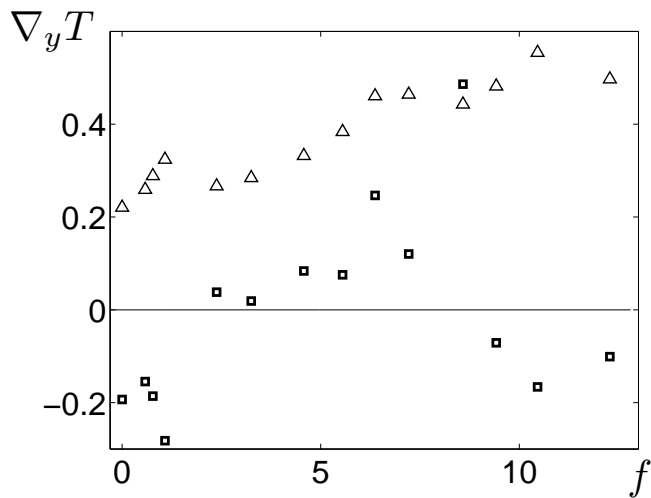


FIG. 4: Horizontal gradient of the mean temperature $\nabla_y T$ (squares) and the amplitude of the nonlinear long-term oscillations of this gradient (triangles) versus the frequency f of the grid oscillations for the unstably stratified turbulent flow. The mean temperature gradient is measured in K cm^{-1} and the frequency f is measured in Hz.

mean temperature.

In order to avoid side effects of the grids we present the experimental results recorded in the central region of the chamber with the size of $10 \times 10 \times 10 \text{ cm}^3$. In Figs. 7-9 we show the frequency dependencies of the following measured turbulence parameters: the turbulent velocity

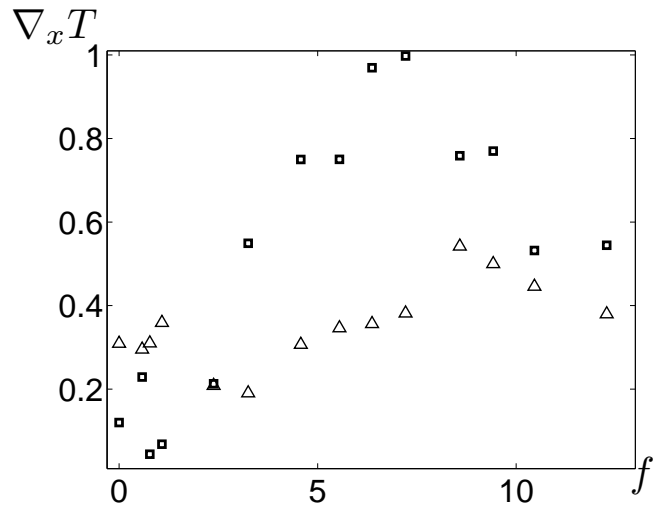


FIG. 5: Horizontal gradient of the mean temperature $\nabla_x T$ (squares) and the amplitude of the nonlinear long-term oscillations of this gradient (triangles) versus the frequency f of the grid oscillations for the unstably stratified turbulent flow. The mean temperature gradient is measured in K cm^{-1} and the frequency f is measured in Hz.

components u_y and u_z , the corresponding integral scales of turbulence along horizontal y and vertical z directions (ℓ_y and ℓ_z) and ratio of the turbulent time scales τ_y/τ_z , where $\tau_y = \ell_y/u_y$ and $\tau_z = \ell_z/u_z$. Inspection of Fig. 8 shows that the turbulent length scales are weakly dependent on the frequency f of the grid oscillations in the unstably stratified turbulent flow for $f > 3$ Hz, while the turbulent velocities and turbulent time scales vary strongly with the frequency f . Note that $\tau_{z,y} f$ tends to a constant (~ 3) for higher frequencies ($f > 5$ Hz) of the forcing.

However, a more careful analysis shows that there are different regimes in unstably stratified flows: when $f < 10$ Hz the behaviour of different turbulent characteristics is not universal (e.g. there is a strong dependence on frequency of the grid oscillations), and a high-frequency range (when $f > 10$ Hz), whereby the behaviour of turbulent characteristics tends to be universal. These features are observed, e.g., in the frequency dependencies of the vertical gradient of the mean temperature $\nabla_z T$ (shown in Fig. 3), and of the non-dimensional ratio $-\ell_z \nabla_z T / \sqrt{\langle \theta^2 \rangle}$ (see Fig. 10), as well as of the ratio of turbulent velocities u_z^*/u_z in isothermal and unstably stratified turbulent flows (shown in Fig. 11). Here u_z^* is the vertical component of the measured turbulent velocity in isothermal turbulence, θ are fluctuations of fluid temperature and T is the mean temperature. On the other hand, the frequency dependence of the r.m.s. of temperature fluctuations, $\sqrt{\langle \theta^2 \rangle}$, does not demonstrate a universal behavior (see Fig. 12). Note that the nontrivial dependence of the temperature fluctuations $\sqrt{\langle \theta^2 \rangle}$ versus the frequency f of the grid oscillations is caused by the nontrivial behaviour

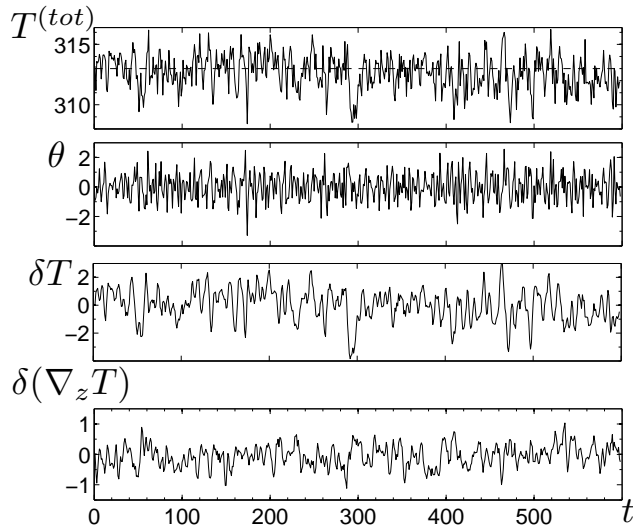


FIG. 6: Time dependencies of the instantaneous temperature T^{tot} , the temperature fluctuations θ , the variations of mean temperature $\delta T = T - \bar{T}$ and the variations of the vertical mean temperature gradient $\delta(\nabla_z T) = \nabla_z T - \overline{\nabla_z T}$ due to the long-term nonlinear oscillations of the mean temperature (with the period ~ 10 s). The bar denotes additional time averaging. These time dependencies are measured in the center of the chamber at the frequency $f = 10$ Hz of the grid oscillations for the unstably stratified turbulent flow. These temperature characteristics are measured in K.

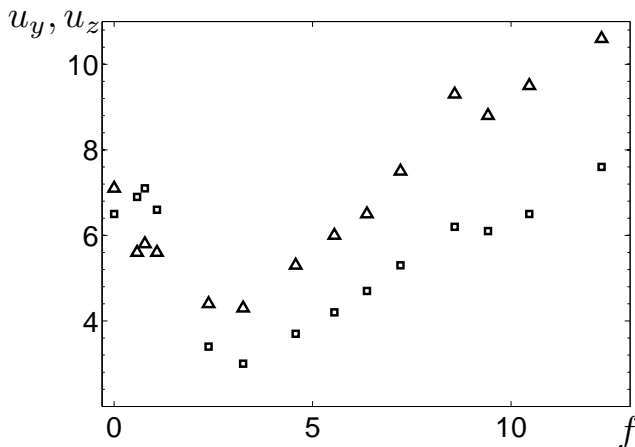


FIG. 7: Components u_y (triangles) and u_z (squares) of the measured turbulent velocity versus the frequency f of the grid oscillations for the unstably stratified turbulent flow. The turbulent velocity is measured in cm s^{-1} and the frequency f is measured in Hz.

of the mean temperature gradients along x, y, z axes (see Figs. 3-5).

In Fig. 11 along with the ratios of turbulent velocities u_z^*/u_z in isothermal and unstably stratified turbulent flows, we also plot the ratio u_z^*/\tilde{u}_z , where \tilde{u}_z is the vertical component of the effective turbulent velocity,

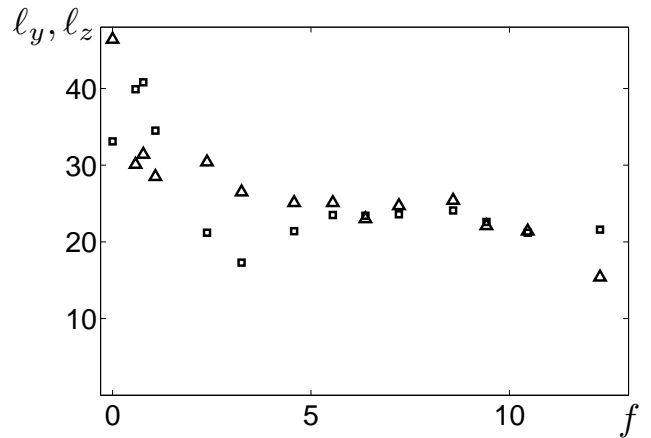


FIG. 8: Horizontal and vertical integral scales of turbulence l_y (triangles) and l_z (squares) versus the frequency f of the grid oscillations for the unstably stratified turbulent flow. The turbulent length scales are measured in mm and the frequency f is measured in Hz.

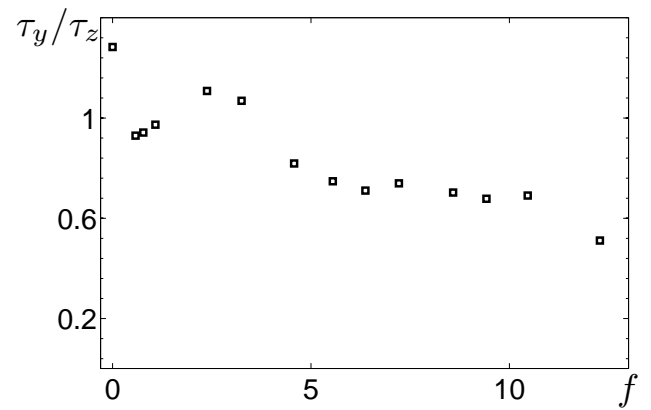


FIG. 9: The ratio of the turbulent time scales $\tau_y = l_y/u_y$ to $\tau_z = l_z/u_z$ versus the frequency f of the grid oscillations for the unstably stratified turbulent flow. The turbulent time scales are measured in s and the frequency f is measured in Hz.

$\tilde{u}_z = [(u_z^*)^2 + 4\ell_z \beta \sqrt{\langle \theta^2 \rangle}]^{1/2}$, $\beta = g/T_*$ is the buoyancy parameter, T_* is a reference value of the mean absolute temperature and \mathbf{g} is the acceleration of gravity. This effective velocity takes into account the production of the turbulence by buoyancy. Inspection of Fig. 11 shows that the values of these ratios are very close. The latter implies that the measured turbulent velocity in the unstably stratified turbulent flow, u_z , is of the order of \tilde{u}_z , i.e.,

$$u_z \simeq [(u_z^*)^2 + 4\ell_z \beta \sqrt{\langle \theta^2 \rangle}]^{1/2}. \quad (1)$$

In the next section we analyze the obtained experimental results.

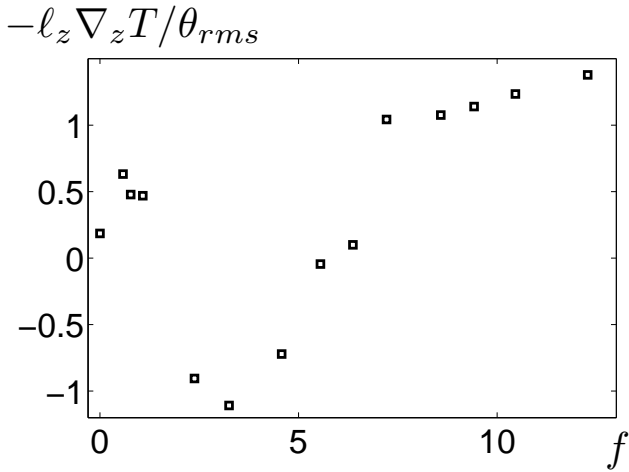


FIG. 10: The non-dimensional ratio $-\ell_z \nabla_z T / \theta_{rms}$ versus the frequency f of the grid oscillations for the unstably stratified turbulent flow, where $\theta_{rms} = \sqrt{\langle \theta^2 \rangle}$.

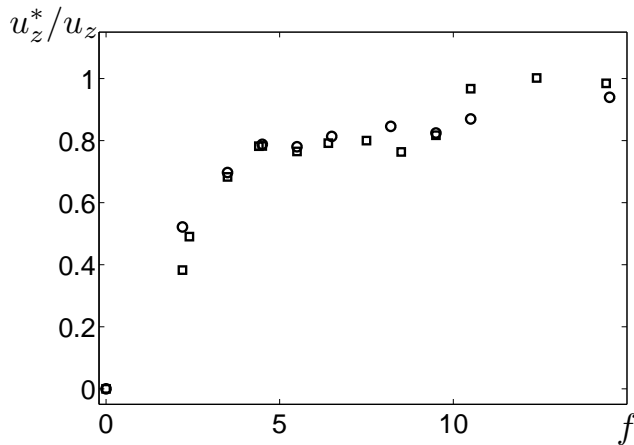


FIG. 11: Ratios u_z^*/u_z (squares) and u_z^*/\tilde{u}_z (circles) of the measured turbulent velocity versus the frequency f of the grid oscillations. Here u_z^* is the vertical component of the measured turbulent velocity in the isothermal turbulence, u_z is the vertical component of the measured turbulent velocity in the unstably stratified turbulent flow, \tilde{u}_z is the vertical component of the effective turbulent velocity, $\tilde{u}_z = [(u_z^*)^2 + 4\ell_z \beta \sqrt{\langle \theta^2 \rangle}]^{1/2}$, that takes into account the production of the turbulence by buoyancy. The turbulent velocity is measured in cm s^{-1} and the frequency f is measured in Hz.

III. THEORETICAL ANALYSIS AND COMPARISON WITH EXPERIMENTAL RESULTS

Let us analyze the frequency dependence of the non-dimensional ratio $\ell_z \nabla_z T / \sqrt{\langle \theta^2 \rangle}$. To this end we consider the budget equation for the temperature fluctu-

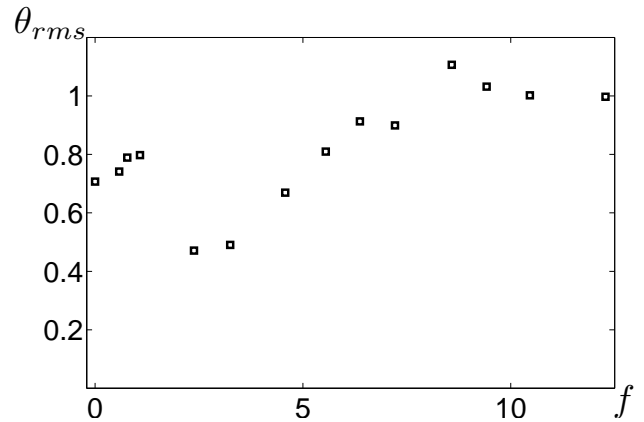


FIG. 12: The r.m.s. of temperature fluctuations $\theta_{rms} = \sqrt{\langle \theta^2 \rangle}$ versus the frequency f of the grid oscillations for the unstably stratified turbulent flow.

ations $E_\theta = \langle \theta^2 \rangle / 2$:

$$\frac{DE_\theta}{Dt} + \text{div } \Phi_\theta = -(\mathbf{F} \cdot \nabla)T - \epsilon_\theta, \quad (2)$$

(see, e.g., [59–61]), where $D/Dt = \partial/\partial t + \mathbf{U} \cdot \nabla$, \mathbf{u} are the fluctuation of the fluid velocity, \mathbf{U} is the mean velocity that describes coherent structure, $\Phi_\theta = (1/2)\langle \mathbf{u} \theta^2 \rangle$ is the third-order moment that determines the flux of E_θ , $F_i = \langle u_i \theta \rangle$ is the turbulent heat flux, θ are the temperature fluctuations, $\epsilon_\theta = E_\theta / (C_\theta \tau_0)$ is the dissipation rate of E_θ , τ_0 is the characteristic turbulent time and C_θ is an empirical constant. In a steady-state Eq. (2) yields:

$$\langle \theta^2 \rangle \approx -2\tau_0 (\mathbf{F} \cdot \nabla)T = 2C_D \ell^2 (\nabla T)^2, \quad (3)$$

where τ_0 is the characteristic turbulent time in the integral scale ℓ of the turbulent motions. In deriving Eq. (3) we take into account that the turbulent heat flux is given by $F_i = -D_T \nabla_i T$, where $D_T = C_D u_0 \ell$ is the turbulent temperature diffusion coefficient and C_D is the non-dimensional constant. We also neglected a small term $\text{div } \Phi_\theta$ in Eq. (2) for nearly homogeneous turbulent convection. Equation (3) implies that the non-dimensional ratio

$$\frac{\ell_z |\nabla_z T|}{\sqrt{\langle \theta^2 \rangle}} = \text{const}, \quad (4)$$

which is in a good agreement with our experimental results for $f > 8$ Hz (see Fig. 10). Equation (4) is in agreement with the corresponding equation derived by means of the path integral approach in [62] for the passive scalar advected by the delta-correlated in time Gaussian smooth velocity field. Equation (4) can be also derived using spectrum of temperature fluctuations found by dimensional arguments in [63] and by the renormalization procedure in [64]. In Appendix we derive Eq. (3) employed in this subsection. In particular, we use two different procedures, namely a quasi-linear approach (or a second

order correlation approximation) that is valid for small Peclet numbers and the spectral τ approximation that is valid for large Peclet numbers.

Now let us discuss the generalization of Eq. (4) for the case when the temperature field cannot be considered as a passive scalar. To this end we use the budget equation for the turbulent heat flux $F_i = \langle u_i \theta \rangle$:

$$\frac{DF_i}{Dt} + \nabla_j \Phi_{ij}^{(F)} = 2\beta_i E_\theta + \frac{1}{\rho} \langle \theta \nabla_i p \rangle - \langle u_i u_j \rangle \nabla_j T - (\mathbf{F} \cdot \nabla) U_i - \epsilon_i^{(F)}, \quad (5)$$

where $\beta_i = \beta e_z$, p are the pressure fluctuations, ρ is the fluid density, \mathbf{U} is the mean velocity, $\epsilon_i^{(F)}$ is the dissipation rate of the turbulent heat flux and $\Phi_{ij}^{(F)} = \langle u_i u_j \theta \rangle + \delta_{ij} \rho^{-1} \langle \theta p \rangle / 2$ is the term that includes the third-order moments. According to the estimate made in [61], $2\beta_i E_\theta + \rho^{-1} \langle \theta \nabla_i p \rangle \approx 4\beta_i E_\theta$. In a steady-state case Eqs. (2) and (5) yield:

$$\frac{\ell_* \nabla_* T}{\sqrt{\langle \theta^2 \rangle}} = \frac{1}{2C_\theta C_F} = \text{const}, \quad (6)$$

where

$$[\ell_* \nabla_* T]^2 = [(\ell_x \nabla_x T)^2 + (\ell_y \nabla_y T)^2 + (\ell_z \nabla_z T)^2] \times [1 + 4C_\theta C_F \beta \tau_0^2 (\nabla_z T)]^{-1}, \quad (7)$$

and C_F is an empirical constant. Here we take into account that the dissipation rate of the turbulent heat flux is $\epsilon_i^{(F)} = F_i / C_F \tau_0$ and $\tau_x \approx \tau_y \approx \tau_z = \tau_0$. In Eqs. (6) and (7) we also have neglected the terms $\sim O(\ell^3 / L_T^3; \ell^3 / (L_T^2 L_U))$, where L_T and L_U are the characteristic spatial scales of the mean temperature and velocity field variations. In Fig. 13 we plot the non-dimensional ratio $\ell_* \nabla_* T / \sqrt{\langle \theta^2 \rangle}$ versus the frequency f of the grid oscillations for the unstably stratified turbulent flow obtained in our experiments, where we assumed that $\ell_x = \ell_y$ and $C_\theta C_F = 1/12$. Inspection of Fig. 13 shows a good agreement between theoretical predictions based on Eq. (7) and the experimental results even in the range of parameters whereby the behaviour of the temperature field is different from that of the passive scalar.

Finally, let us derive Eq. (1) for the measured turbulent velocity in the unstably stratified turbulent flow. We use the budget equation for the turbulent kinetic energy $E_K = \langle \mathbf{u}^2 \rangle / 2$:

$$\frac{DE_K}{Dt} + \text{div} \Phi_K = -\langle u_i u_j \rangle \nabla_j U_i + \beta F_z + \langle \mathbf{u} \cdot \mathbf{f}_f \rangle - \varepsilon, \quad (8)$$

where $\Phi_K = \rho^{-1} \langle \mathbf{u} p \rangle + (1/2) \langle \mathbf{u} u^2 \rangle$ is the term that includes the third-order moments, $\langle \mathbf{u} \cdot \mathbf{f}_f \rangle$ is the production of turbulence caused by the grid oscillations. In the steady-state Eq. (8) yields $\langle \mathbf{u}^2 \rangle = 2\tau_0 [\nu_T S^2 + \langle \mathbf{u} \cdot \mathbf{f}_f \rangle + \beta F_z]$, where ν_T is the turbulent viscosity. Let us introduce the characteristic velocity for isothermal turbulence

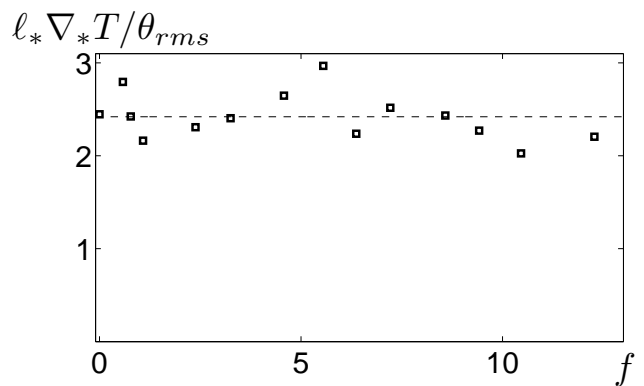


FIG. 13: The non-dimensional ratio $\ell_* \nabla_* T / \theta_{rms}$ versus the frequency f of the grid oscillations for the unstably stratified turbulent flow, where $\theta_{rms} = \sqrt{\langle \theta^2 \rangle}$.

$(\mathbf{u}^*)^2 = 2\tau_0 [\nu_T S_*^2 + \langle \mathbf{u} \cdot \mathbf{f}_f \rangle]$, where S_* is the large-scale shear that can appear in isothermal oscillating grid turbulence. Note that for larger frequencies of the grid oscillations the large-scale circulations caused by turbulent convection disappear and $S \rightarrow S_*$. Since for large frequencies of the grid oscillations the turbulent heat flux $F_z = -D_T \nabla_z T$ and $|\nabla_z T| \simeq \sqrt{\langle \theta^2 \rangle} / \ell$ [see Eq. (3) and Fig. 10], we arrive at Eq. (1). Here we take into account that $\mathbf{u}_h^2 \simeq (\mathbf{u}_h^*)^2$ for the horizontal component of the turbulent velocity.

We have also checked experimental results (but not systematically) at smaller temperature difference $\Delta T = 25$ K between the top and bottom walls (i.e., smaller Ra), and found only minor changes in the final results. Note also that in the case of large frequencies of the grid oscillations, i.e., in the limiting regime of the unstably stratified turbulent flow without the LSC, whereby the temperature field behaves like a passive scalar, the constant C_D is nearly independent of the molecular heat transport coefficients for large Peclet numbers (which correspond to the conditions of our experiments). The constant C_D depends on the molecular heat transport coefficients only for small Peclet numbers (see Appendix).

Note that the turbulent convection studied in our experiments is non-Boussinesq, i.e., $\text{div} \mathbf{u} \neq 0$. In the theoretical analysis we use the anelastic approximation, $\text{div} (\rho \mathbf{u}) = 0$. It should be noted that the deviation from the Boussinesq approximation in our experiments is less than 10 % (i.e., spatial variations of the fluid density are $\delta\rho/\rho < 0.1$).

IV. DISCUSSION AND CONCLUSIONS

In the present study we have investigated transition phenomena caused by the external forcing from Rayleigh-Bénard convection with LSC to the limiting regime of unstably stratified turbulent flow without LSC, whereby

the temperature field behaves like a passive scalar. The external forcing of turbulence is produced by two oscillating grids. When the frequency of the grid oscillations is larger than 2 Hz, the large-scale circulation (LSC) in the yz -plane in turbulent convection is destroyed. On the other hand, a complicated mean flow of the spiral form in the xz -plane with a non-zero mean vorticity in the y direction exists when the frequencies of the grid oscillations $2 < f < 7$ Hz. The destruction of the LSC is accompanied by a strong change of the mean temperature distribution. In the central part of the flow the vertical mean temperature gradient changes its direction depending on the frequency of the grid oscillations.

We have demonstrated that the production of temperature fluctuations in a forced turbulent convection is caused by tangling of the mean temperature gradient by the velocity fluctuations. In particular, the observed constant ratio $(2\ell_z \nabla_z T)^2 / \langle \theta^2 \rangle$ for large frequencies of the grid oscillations is typical for this mechanism of generation of temperature fluctuations. We have generalized this result for all regimes of the unstably stratified turbulent flow whereby the ratio $[(\ell_x \nabla_x T)^2 + (\ell_y \nabla_y T)^2 + (\ell_z \nabla_z T)^2] / \langle \theta^2 \rangle$ varies slightly even in the range of parameters whereby the behaviour of the temperature field is different from that of the passive scalar. The experimental results obtained in this study are in a good agreement with theoretical predictions based on the budget equations for turbulent kinetic energy, turbulent temperature fluctuations and turbulent heat flux.

We have also found that in unstably stratified turbulent flow the vertical component of the turbulent velocity field is determined by Eq. (1). The latter equation is derived from the balance equation for the turbulent kinetic energy. This implies that the buoyancy heat flux strongly contributes to the production of the turbulent kinetic energy in turbulent convection in the absence of the LSC. However, the turbulent kinetic energy in large Rayleigh number turbulent convection with coherent structures (LSC) is produced by shear, rather than by buoyancy (see [40]).

Appendix A: Temperature fluctuations

Evolution of a temperature field $T_{\text{tot}}(t, \mathbf{r})$ in a turbulent flow is determined by the following equation:

$$\frac{\partial T_{\text{tot}}}{\partial t} + (\hat{\mathbf{v}} \cdot \nabla) T_{\text{tot}} + (\gamma - 1) (\nabla \cdot \hat{\mathbf{v}}) T_{\text{tot}} = D \nabla^2 T_{\text{tot}}, \quad (\text{A1})$$

where D is the coefficient of molecular temperature diffusion, $\gamma = c_p/c_v$ is the ratio of specific heats, $\hat{\mathbf{v}}$ is the velocity field that satisfies to continuity equation in anelastic approximation for a low-Mach-number flow:

$$\nabla \cdot (\rho \hat{\mathbf{v}}) = 0. \quad (\text{A2})$$

Combining Eq. (A1) and (A2) we obtain the following equation:

$$\frac{\partial T_{\text{tot}}}{\partial t} + (\mathbf{v} \cdot \nabla) T_{\text{tot}} = D \nabla^2 T_{\text{tot}}, \quad (\text{A3})$$

where $\mathbf{v} = \gamma \hat{\mathbf{v}}$ and we take into account that for a low-Mach-number flow without imposed external pressure gradient $\nabla \rho / \rho \approx -\nabla T_{\text{tot}} / T_{\text{tot}}$.

Averaging Eq. (A3) over ensemble of turbulent velocity field we obtain the equation for the evolution of the mean temperature field $T(t, \mathbf{r})$:

$$\frac{\partial T}{\partial t} + (\mathbf{U} \cdot \nabla) T + \nabla \cdot \mathbf{F} = D \nabla^2 T, \quad (\text{A4})$$

where $\mathbf{U} = \gamma \hat{\mathbf{U}}$, $\hat{\mathbf{U}}$ is the mean fluid velocity, $\mathbf{F} = \langle \mathbf{u} \theta \rangle$ is the heat flux, $\mathbf{u} = \gamma \hat{\mathbf{u}}$ and $\hat{\mathbf{u}}$ are the velocity fluctuations.

1. Temperature fluctuations for small Peclet numbers

In order to study temperature fluctuations for small Peclet numbers we use a quasi-linear approach or a second order correlation approximation (see, e.g., [65]). Subtracting Eq. (A4) from Eq. (A3) yields equation for the temperature fluctuations:

$$\frac{\partial \theta}{\partial t} + Q - D \nabla^2 \theta = I, \quad (\text{A5})$$

where $I = -(\mathbf{u} \cdot \nabla) T$ is the source term and $Q = \nabla \cdot [\mathbf{u} \theta - \langle \mathbf{u} \theta \rangle] + \theta (\mathbf{u} \cdot \nabla) \rho / \rho$ is the nonlinear term. In the expression for Q we neglected the term $\langle \theta \mathbf{u} \rangle \cdot \nabla \rho / \rho$ which is quadratic in large-scale spatial derivative. Let us neglect the nonlinear term but keep the molecular diffusion term in Eq. (A5). For this reason this approach is called a quasi-linear or perturbation approach. This approximation for a given velocity field is valid only for small Peclet numbers ($\text{Pe} \ll 1$), where $\text{Pe} = u_0 \ell / D$. Let us rewrite Eq. (A5) in a Fourier space. Then the solution of Eq. (A5) is given by $\theta(\omega, \mathbf{k}) = G_D(\omega, \mathbf{k}) I(\omega, \mathbf{k})$, where $G_D(\omega, \mathbf{k}) = (Dk^2 + i\omega)^{-1}$.

Let us apply a standard two-scale approach, whereby the non-instantaneous two-point second-order correlation function is written as follows:

$$\begin{aligned} \langle u_i(t_1, \mathbf{x}) \theta(t_2, \mathbf{y}) \rangle &= \int \langle u_i(\omega_1, \mathbf{k}_1) \theta(\omega_2, \mathbf{k}_2) \rangle \exp[i(\mathbf{k}_1 \cdot \mathbf{x} \\ &+ \mathbf{k}_2 \cdot \mathbf{y}) + i(\omega_1 t_1 + \omega_2 t_2)] d\omega_1 d\omega_2 d\mathbf{k}_1 d\mathbf{k}_2 \\ &= \int F_i(\omega, \mathbf{k}) \exp[i\mathbf{k} \cdot \mathbf{r} + i\omega \tilde{\tau}] d\omega d\mathbf{k}, \end{aligned} \quad (\text{A6})$$

where we use large scale variables: $\mathbf{R} = (\mathbf{x} + \mathbf{y})/2$, $\mathbf{K} = \mathbf{k}_1 + \mathbf{k}_2$, $t = (t_1 + t_2)/2$, $\Omega = \omega_1 + \omega_2$, and small scale variables: $\mathbf{r} = \mathbf{x} - \mathbf{y}$, $\mathbf{k} = (\mathbf{k}_1 - \mathbf{k}_2)/2$, $\tilde{\tau} = t_1 - t_2$, $\omega = (\omega_1 - \omega_2)/2$,

$$\begin{aligned} F_i(\omega, \mathbf{k}) &= \int \langle u_i(\omega_1, \mathbf{k}_1) \theta(\omega_2, \mathbf{k}_2) \rangle \exp[i\Omega t \\ &+ i\mathbf{K} \cdot \mathbf{R}] d\Omega d\mathbf{K}, \end{aligned} \quad (\text{A7})$$

and $\omega_1 = \omega + \Omega/2$, $\omega_2 = -\omega + \Omega/2$, $\mathbf{k}_1 = \mathbf{k} + \mathbf{K}/2$, $\mathbf{k}_2 = -\mathbf{k} + \mathbf{K}/2$ (see, e.g., [66]). We assume here that there exists a separation of scales, i.e., the maximum scale of random motions ℓ is much smaller than the characteristic scales of inhomogeneities of the mean temperature and fluid density.

The turbulent heat flux F_i and the function E_θ are given by the following relations:

$$F_i = \int \langle u_i(\omega, \mathbf{k}) I(-\omega, -\mathbf{k}) \rangle G_D(-\omega, -\mathbf{k}) d\omega d\mathbf{k}, \quad (\text{A8})$$

$$E_\theta = \int \langle \theta(\omega, \mathbf{k}) I(-\omega, -\mathbf{k}) \rangle G_D(-\omega, -\mathbf{k}) d\omega d\mathbf{k}. \quad (\text{A9})$$

Hereafter we use the simple model for the second moments of a random velocity field, $\langle u_i(\omega, \mathbf{k}) u_j(-\omega, -\mathbf{k}) \rangle$, and the velocity-temperature fluctuations, $\langle \theta(\omega, \mathbf{k}) u_j(-\omega, -\mathbf{k}) \rangle$, in a Fourier space:

$$\langle u_i(\omega, \mathbf{k}) u_j(-\omega, -\mathbf{k}) \rangle = \frac{\gamma^2 u_0^2 E(k)}{8\pi k^2} \left[\delta_{ij} - \frac{k_i k_j}{k^2} \right] \delta(\omega), \quad (\text{A10})$$

$$\langle \theta(\omega, \mathbf{k}) u_i(-\omega, -\mathbf{k}) \rangle = \frac{3F_z E(k)}{8\pi k^2} e_m P_{im}(k) \delta(\omega), \quad (\text{A11})$$

where $\delta(\omega)$ is the Dirac's delta-function, δ_{ij} is the Kronecker tensor, $P_{ij}(k) = \delta_{ij} - k_i k_j / k^2$, the energy spectrum function is $E(k) = k_0^{-1} (q-1) (k/k_0)^{-q}$, the exponent $1 < q < 3$, the wave number $k_0 = 1/\ell$, the length ℓ is the maximum scale of random motions and u_0 is the characteristic velocity in the maximum scale of random motions. After integration in ω -space and in \mathbf{k} -space, Eqs. (A8) and (A9) yield formulae for the turbulent heat flux F_i and the temperature fluctuation function E_θ :

$$F_i = -D_T \nabla_i T, \quad D_T = C_D u_0 \ell, \quad (\text{A12})$$

$$E_\theta = -\frac{3C_D}{\gamma^2} \tau_0 (\mathbf{F} \cdot \nabla) T, \quad (\text{A13})$$

$$C_D = \frac{(q-1)\gamma^2}{3(q+1)} \text{Pe}, \quad (\text{A14})$$

where D_T is the turbulent temperature diffusion coefficient. Equations (A12)-(A14) also can be obtained using spectrum of temperature fluctuations for small Peclet numbers found by means of dimensional arguments in [67] and by the Lagrangian-history direct-interaction approximation applied in [68].

2. Temperature fluctuations for large Peclet numbers

In this subsection we derive formulae for the turbulent heat flux F_i and the temperature fluctuation function E_θ using the τ approach that is valid for large Peclet and Reynolds numbers. Using Eq. (A5) written in a Fourier space we derive equation for the instantaneous

two-point second-order correlation functions $F_i(t, \mathbf{k}) = \langle u_i(t, \mathbf{k}) \theta(t, -\mathbf{k}) \rangle$ and $E_\theta(t, \mathbf{k}) = (1/2) \langle \theta(t, \mathbf{k}) \theta(t, -\mathbf{k}) \rangle$:

$$\frac{dF_i}{dt} = \langle u_i(t, \mathbf{k}) I(t, -\mathbf{k}) \rangle + \hat{\mathcal{M}}F_i^{(III)}(\mathbf{k}), \quad (\text{A15})$$

$$\frac{dE_\theta}{dt} = \langle \theta(t, \mathbf{k}) I(t, -\mathbf{k}) \rangle + \hat{\mathcal{M}}E_\theta^{(III)}(\mathbf{k}), \quad (\text{A16})$$

where $\hat{\mathcal{M}}F_i^{(III)}(\mathbf{k}) = -[\langle u_i Q \rangle + \langle (\partial u_i / \partial t) \theta \rangle - D \langle u_i \nabla^2 \theta \rangle]_{\mathbf{k}}$ and $\hat{\mathcal{M}}E_\theta^{(III)}(\mathbf{k}) = -(1/2) [\langle \theta Q \rangle - D \langle \theta \nabla^2 \theta \rangle]_{\mathbf{k}}$ are the third-order moment terms appearing due to the nonlinear terms which include also molecular diffusion term.

The equation for the second moment includes the first-order spatial differential operators $\hat{\mathcal{M}}$ applied to the third-order moments $F^{(III)}$. A problem arises how to close the system, i.e., how to express the third-order terms $\hat{\mathcal{M}}F^{(III)}$ through the lower moments $F^{(II)}$ (see, e.g., [69–71]). We use the spectral τ approximation which postulates that the deviations of the third-moment terms, $\hat{\mathcal{M}}F^{(III)}(\mathbf{k})$, from the contributions to these terms afforded by the background turbulence, $\hat{\mathcal{M}}F^{(III,0)}(\mathbf{k})$, can be expressed through the similar deviations of the second moments, $F^{(II)}(\mathbf{k}) - F^{(II,0)}(\mathbf{k})$:

$$\begin{aligned} & \hat{\mathcal{M}}F^{(III)}(\mathbf{k}) - \hat{\mathcal{M}}F^{(III,0)}(\mathbf{k}) \\ &= -\frac{1}{\tau_r(k)} \left[F^{(II)}(\mathbf{k}) - F^{(II,0)}(\mathbf{k}) \right], \end{aligned} \quad (\text{A17})$$

(see, e.g., [69, 72, 73]), where $\tau_r(k)$ is the scale-dependent relaxation time, which can be identified with the correlation time $\tau(k)$ of the turbulent velocity field for large Reynolds and Peclet numbers. The functions with the superscript (0) correspond to the background turbulence with a zero gradient of the mean temperature. Validation of the τ approximation for different situations has been performed in numerous numerical simulations and analytical studies (see, e.g., review [74]; and also discussion in [73], Sec. 6).

Note that the contributions of the terms with the superscript (0) vanish because when the gradient of the mean temperature is zero, the turbulent heat flux and the temperature fluctuations vanish. Consequently, Eq. (A17) for $\hat{\mathcal{M}}F_i^{(III)}(\mathbf{k})$ reduces to $\hat{\mathcal{M}}F_i^{(III)}(\mathbf{k}) = -F_i(\mathbf{k})/\tau(k)$ and for $\hat{\mathcal{M}}E_\theta^{(III)}(\mathbf{k}) = -E_\theta(\mathbf{k})/\tau(k)$. We also assume that the characteristic time of variation of the second moments $F_i(\mathbf{k})$ and $E_\theta(\mathbf{k})$ are substantially larger than the correlation time $\tau(k)$ for all turbulence scales. Therefore, in a steady-state Eqs. (A15) and (A16) yield the following formulae for the turbulent heat flux F_i and the function E_θ :

$$F_i = \int \tau(k) \langle u_i(t, \mathbf{k}) I(t, -\mathbf{k}) \rangle d\mathbf{k}, \quad (\text{A18})$$

$$E_\theta = \int \tau(k) \langle \theta(t, \mathbf{k}) I(t, -\mathbf{k}) \rangle d\mathbf{k}. \quad (\text{A19})$$

Now we use the following simple model for the second moments of turbulent velocity field, $\langle u_i(\mathbf{k}) u_j(-\mathbf{k}) \rangle$ and

the velocity-temperature fluctuations, $\langle \theta(\mathbf{k}) u_j(-\mathbf{k}) \rangle$, in \mathbf{k} space:

$$\langle u_i(\mathbf{k}) u_j(-\mathbf{k}) \rangle = \frac{\gamma^2 u_0^2 E(k)}{8\pi k^2} \left[\delta_{ij} - \frac{k_i k_j}{k^2} \right], \quad (\text{A20})$$

$$\langle \theta(\mathbf{k}) u_i(-\mathbf{k}) \rangle = \frac{3F_z E(k)}{8\pi k^2} e_m P_{im}(k). \quad (\text{A21})$$

After integration in \mathbf{k} -space Eqs. (A18) and (A19) we arrive at equations for the turbulent heat flux, F_i , and the temperature fluctuations, E_θ :

$$F_i = -D_T \nabla_i T, \quad D_T = C_D u_0 \ell, \quad (\text{A22})$$

$$E_\theta = -\tau_0 (\mathbf{F} \cdot \nabla) T, \quad C_D = \gamma^2 / 3. \quad (\text{A23})$$

In the derivation we used the following expression for the turbulent correlation time, $\tau(k) = 2\tau_0 (k/k_0)^{1-q}$, where $\tau_0 = \ell/u_0$ is the characteristic turbulent time. Therefore, the formulae for the turbulent heat flux F_i and the function E_θ are similar for small and large Peclet numbers, while the coefficients are different in these two cases. Notably, the theoretical predictions for large Peclet number

(which correspond to the laboratory experiments) are in agreement with experimental results and with the estimate based on the balance equation for E_θ [see Eq. (3)]. Equations (A22) and (A23) are in agreement with the corresponding equations derived by means of the path integral approach in [62] for the passive scalar advected by the delta-correlated in time Gaussian smooth velocity field. Equations (A22) and (A23) also can be obtained using spectrum of temperature fluctuations found by means of dimensional arguments in [63] and by the renormalization procedure for large Peclet numbers performed in [64].

Acknowledgments

We thank A. Krein for his assistance in construction of the experimental set-up. This research was supported in part by the Israel Science Foundation governed by the Israeli Academy of Sciences (Grant 259/07).

-
- [1] D. Etling and R. A. Brown, *Boundary-Layer Meteorol.* **65**, 215 (1993).
- [2] B. W. Atkinson and J. Wu Zhang, *Rev. Geophys.* **34**, 403 (1996).
- [3] S. S. Zilitinkevich, *Turbulent Penetrative Convection* (Avebury Technical, Aldershot, 1991).
- [4] T. Elperin, N. Kleeorin, I. Rogachevskii and S.S. Zilitinkevich, *Boundary-Layer Meteorology* **119**, 449-472 (2006).
- [5] R. Krishnamurti and L. N. Howard, *Proc. Natl.Acad. Sci. USA* **78**, 1981 (1981).
- [6] M. Sano, X. Z. Wu and A. Libchaber, *Phys. Rev. A* **40**, 6421 (1989).
- [7] A. Tilgner, A. Belmonte and A. Libchaber, *Phys. Rev. E* **47**, R2253 (1993).
- [8] S. Ciliberto, S. Cioni and C. Laroche, *Phys. Rev. E* **54**, R5901 (1996).
- [9] J. J. Niemela, L. Skrbek, K. R. Sreenivasan and R. J. Donnelly, *J. Fluid Mech.* **449**, 169 (2001).
- [10] K. R. Sreenivasan, A. Bershadskii, and J. J. Niemela, *Phys. Rev. E* **65**, 056306 (2002).
- [11] J. J. Niemela and K. R. Sreenivasan, *Europhys. Lett.* **62**, 829 (2003).
- [12] X.-L. Qiu and P. Tong, *Phys. Rev. E* **64**, 036304 (2001).
- [13] K.-Q. Xia, S. Lam, and S.-Q. Zhou, *Phys. Rev. Lett.* **88**, 064501 (2002).
- [14] U. Burr, W. Kinzelbach, A. Tsinober, *Phys. Fluids* **15**, 2313 (2003).
- [15] K.-Q. Xia, C. Sun, and S.-Q. Zhou, *Phys. Rev. E* **68**, 066303 (2003).
- [16] A. Liberzon, B. Lüthi, M. Guala, W. Kinzelbach and A. Tsinober, *Phys. Fluids* **17**, 095110 (2005).
- [17] H.-D. Xi, S. Lam and K.-Q. Xia, *J. Fluid Mech.* **503**, 47 (2004).
- [18] X. D. Shang, X. L. Qiu, P. Tong and K.-Q. Xia, *Phys. Rev. E* **70**, 026308 (2004).
- [19] D. Funfschilling and G. Ahlers, *Phys. Rev. Lett.* **92**, 194502 (2004); D. Funfschilling, E. Brown and G. Ahlers, *J. Fluid Mech* **607**, 119 (2008).
- [20] E. Brown, A. Nikolaenko and G. Ahlers, *Phys. Rev. Lett.* **95**, 084503 (2005).
- [21] J. Verdoold, M. J. Tummers and K. Hanjalić, *Phys. Rev. E* **73**, 056304 (2006).
- [22] A. Eidelman, T. Elperin, N. Kleeorin, A. Markovich and I. Rogachevskii, *Experim. Fluids* **40**, 723 (2006).
- [23] C. Resagk, R. du Puits, A. Thess, F. V. Dolzhansky, S. Grossmann, F. F. Araujo, and D. Lohse, *Phys. Fluids* **18**, 095105 (2006).
- [24] E. Brown and G. Ahlers, *J. Fluid Mech.* **568**, 351 (2006); *Phys. Fluids* **18**, 125108 (2006); *Phys. Rev. Lett.* **98**, 134501 (2007); *Phys. Fluids* **20**, 105105, 075101 (2008); *J. Fluid Mech.* **638**, 383 (2009).
- [25] Y. Gasteuil, W. L. Shew, M. Gibert, F. Chillä, B. Castaing and J.-F. Pinton, *Phys. Rev. Lett.* **99**, 234302 (2007).
- [26] H.-D. Xi and K.-Q. Xia, *Phys. Rev. E* **75**, 066307 (2007); *Phys. Fluids* **20**, 055104 (2008).
- [27] H.-D. Xi, S.-Q. Zhou, Q. Zhou, T.-S. Chan and K.-Q. Xia, *Phys. Rev. Lett.* **102**, 044503 (2009); Q. Zhou, H.-D. Xi, S.-Q. Zhou, C. Sun and K.-Q. Xia, *J. Fluid Mech.* **630**, 367 (2009).
- [28] R. du Puits, C. Resagk and A. Thess, *Phys. Rev. E* **80**, 036318 (2009).
- [29] X. He and P. Tong, *Phys. Rev. E* **79**, 026306 (2009).
- [30] G. Ahlers, D. Funfschilling and E. Bodenschatz, *New J. Phys.* **11**, 123001 (2009); D. Funfschilling, E. Bodenschatz and G. Ahlers, *Phys. Rev. Lett.* **103**, 024503 (2009).
- [31] R. M. Kerr, *Phys. Rev. Lett.* **87**, 244502 (2001).
- [32] T. Hartlep, A. Tilgner and F. H. Busse, *Phys. Rev. Lett.* **91**, 064501 (2003).
- [33] A. Parodi, J. von Hardenberg, G. Passoni, A. Provenzale

- and E. A. Spiegel, *Phys. Rev. Lett.* **92**, 194503 (2004).
- [34] M. van Reeuwijk, H. J. J. Jonker and K. Hanjalić, *Phys. Fluids* **17**, 051704 (2005).
- [35] T. Elperin, N. Kleeorin, I. Rogachevskii and S.S. Zilitinkevich, *Phys. Rev. E* **66**, 066305 (2002).
- [36] T. Elperin, I. Golubev, N. Kleeorin and I. Rogachevskii, *Phys. Fluids* **18**, 126601 (2006).
- [37] E. Siggia, *Annu. Rev. Fluid Mech.* **26**, 137 (1994).
- [38] L. P. Kadanoff, *Phys. Today* **54**, 34 (2001).
- [39] G. Ahlers, S. Grossmann and D. Lohse, *Rev. Modern. Phys.* **81**, 503 (2009).
- [40] M. Bukai, A. Eidelman, T. Elperin, N. Kleeorin, I. Rogachevskii and I. Sapir-Katiraie, *Phys. Rev. E* **79**, 066302 (2009).
- [41] T. H. Solomon and J. P. Gollub, *Phys. Rev. Lett.* **64**, 2382 (1990); *Phys. Rev. A* **43**, 6683 (1991).
- [42] S. Ashkenazi and V. Steinberg, *Phys. Rev. Lett.* **83**, 3641 (1999); **83**, 4760 (1999).
- [43] D. Lohse and K.-Q. Xia, *Annu. Rev. Fluid Mech.* **42**, 335 (2010), and referencies therein.
- [44] X.-L. Jin and K.-Q. Xia, *J. Fluid Mech.* **606**, 133 (2008).
- [45] J. Buchholz, A. Eidelman, T. Elperin, G. Grünefeld, N. Kleeorin, A. Krein, I. Rogachevskii, *Experim. Fluids* **36**, 879 (2004).
- [46] M. Gibert, H. Pabiou, F. Chillà and B. Castaing, *Phys. Rev. Lett.* **96**, 084501 (2006).
- [47] M. Gibert, H. Pabiou, J.-C. Tisserand, B. Gertjerenken, B. Castaing and F. Chillà, *Phys. Fluids* **21**, 035109 (2009).
- [48] A. Eidelman, T. Elperin, N. Kleeorin, A. Krein, I. Rogachevskii, J. Buchholz, G. Grünefeld, *Nonl. Proc. Geophys.* **11**, 343 (2004).
- [49] A. Eidelman, T. Elperin, N. Kleeorin, I. Rogachevskii and I. Sapir-Katiraie, *Experim. Fluids* **40**, 744 (2006).
- [50] A. Eidelman, T. Elperin, N. Kleeorin, A. Markovich and I. Rogachevskii, *Nonl. Proc. Geophys.* **13**, 109 (2006).
- [51] J. Baldyga and J. R. Bourne, *Turbulent Mixing and Chemical Reactions* (Wiley, New York, 1999).
- [52] C. T. Crowe, M. Sommerfeld and Y. Tsuji, *Multiphase Flows with Particles and Droplets* (CRC Press, New York, 1998).
- [53] G. L. Borman and K. W. Ragland, *Combustion Engineering*, (MacGraw-Hill, Boston-New-York, 1999).
- [54] R. J. Adrian, *Annu. Rev. Fluid Mech.* **23**, 261 (1991).
- [55] M. Raffel, C. Willert, S. Werely and J. Kompenhans, *Particle Image Velocimetry* (Springer, Berlin-Heidelberg, 2007).
- [56] J. Westerweel, *Experim. Fluids* **29**, S3 (2000).
- [57] T. Elperin, N. Kleeorin and I. Rogachevskii, *Phys. Rev. Lett.* **76**, 224 (1996); **80**, 69 (1998); **81**, 2898 (1998).
- [58] T. Elperin, N. Kleeorin, I. Rogachevskii and D. Sokoloff, *Phys. Rev. E* **61**, 2617 (2000); **64**, 026304 (2001).
- [59] J. C. Kaimal and J. J. Fennigan, *Atmospheric Boundary Layer Flows* (Oxford University Press, New York, 1994).
- [60] Y. Cheng, V. M. Canuto and A. M. Howard, *J. Atmosph. Sci.* **59**, 1550 (2002).
- [61] S. S. Zilitinkevich, T. Elperin, N. Kleeorin and I. Rogachevskii, *Boundary-Layer Meteorology* **125**, 167 (2007).
- [62] T. Elperin, N. Kleeorin and I. Rogachevskii, *Phys. Rev. E* **52**, 2617 (1995).
- [63] A. D. Wheelon, *J. Geophys. Res.* **63**, 849 (1958).
- [64] T. Elperin, N. Kleeorin and I. Rogachevskii, *Phys. Rev. E* **53**, 3431 (1996).
- [65] H. K. Moffatt, *Magnetic Field Generation in Electrically Conducting Fluids* (Cambridge University Press, New York, 1978).
- [66] P. H. Roberts and A. M. Soward, *Astron. Nachr.* **296**, 49 (1975).
- [67] G. K. Batchelor, I. D. Howells and A. A. Townsend, *J. Fluid Mech.* **5**, 134 (1959).
- [68] R. H. Kraichnan, *Phys. Fluids* **11**, 945 (1968).
- [69] S. A. Orszag, *J. Fluid Mech.* **41**, 363 (1970).
- [70] A. S. Monin and A. M. Yaglom, *Statistical Fluid Mechanics* (MIT Press, Cambridge, Massachusetts, 1975), Vol. 2.
- [71] W. D. McComb, *The Physics of Fluid Turbulence* (Clarendon, Oxford, 1990).
- [72] A. Pouquet, U. Frisch, and J. Leorat, *J. Fluid Mech.* **77**, 321 (1976).
- [73] I. Rogachevskii and N. Kleeorin, *Phys. Rev. E* **76**, 056307 (2007).
- [74] A. Brandenburg and K. Subramanian, *Phys. Rept.* **417**, 1 (2005).